Variational Ground-State Quantum Adiabatic Theorem

Bojan Žunkovič,[1,*] Pietro Torta,[2,3] Giovanni Pecci,[4] Guglielmo Lami,[5] and Mario Collura[3,6]
[1]*University of Ljubljana, Faculty of Computer and Information Science, Večna pot 113, 1000 Ljubljana, Slovenia*
[2]*Dipartimento di Fisica, Università degli Studi di Milano, Via Celoria 16, 20133 Milano, Italy*
[3]*SISSA, Via Bonomea 265, I-34136 Trieste, Italy*
[4]*CNR-IOM, Via Bonomea 265, I-34136 Trieste, Italy*
[5]*Laboratoire de Physique Théorique et Modélisation, CNRS UMR 8089, CY Cergy Paris Université, 95302 Cergy-Pontoise Cedex, France*
[6]*INFN Sezione di Trieste, via Bonomea 265, I-34136 Trieste, Italy*

(Received 28 June 2024; accepted 6 February 2025; published 31 March 2025)

We present a variational quantum adiabatic theorem, which states that, under certain assumptions, the adiabatic dynamics projected onto a variational manifold follow the instantaneous variational ground state. We focus on low-entanglement variational manifolds and target Hamiltonians with classical ground states. Despite highly entangled intermediate states along the exact adiabatic path, the variational evolution converges to the target ground state. We demonstrate this approach with several examples that align with our theoretical analysis.

DOI: 10.1103/PhysRevLett.134.130601

Introduction—Adiabatic quantum computation (AQC) is a computational paradigm that relies on a slow continuous change from an initial Hamiltonian H_0 to a final Hamiltonian H_1 over a total annealing time T. The adiabatic theorem [1] ensures that if the initial state is the ground state of H_0 and the evolution is sufficiently slow, the final state approximates the ground state of H_1. By strategically selecting H_1, we can ensure that its ground state serves as a solution to a specific computational problem. Generally, AQC is polynomially equivalent to gate-based quantum computation and thereby universal [2,3]. A relevant subclass of AQC protocols using stoquastic Hamiltonians addresses classical optimization problems and has been proposed as a quantum version of thermal annealing, with quantum fluctuations replacing thermal fluctuations [4]. This quantum annealing formulation is compatible with hardware platforms [5] and holds significant promise for technological applications [6].

The classical simulation of quantum annealing relies on simulated quantum annealing based on path-integral Monte Carlo [7] sampling. Promising results were recently obtained by extending time-dependent Monte Carlo to time-dependent Hamiltonians [8]. However, the actual need for quantum resources and the classical simulability of quantum protocols [9] remain largely unanswered, with the potential to lead to effective quantum-inspired algorithms [10–14], often based on tensor network techniques [15–17].

We take a step in this direction by showing that an effective evolution constrained in a low-entanglement manifold can, under certain conditions, faithfully replace a fully quantum adiabatic evolution if the initial and final (target) states are classical. Our approach helps to elucidate the role of entanglement in quantum annealing. Recent numerical works [18,19] found that, under certain conditions, restricting the accessible Hilbert space to a variational manifold with low entanglement, might even increase the probability of finding the target state, potentially acting as a regularization technique. Indeed, while entanglement is necessary for general quantum computation, its role in quantum optimization is unclear. A similar observation has been made in a related optimization strategy, namely the quantum approximate optimization algorithm [20–22], which has recently shown the possibility of a quantum scaling advantage [23].

The rest of this Letter presents the physical intuition behind the variational ground-state quantum adiabatic evolution and several examples.

Variational ground-state quantum adiabatic theorem—Consider a parametrized Hamiltonian $H(s)$ interpolating between the initial Hamiltonian $H(0) = H_0$, and the final *target* Hamiltonian $H(1) = H_1$. Let us denote the duration of the protocol (annealing time) as T and interpret $s = t/T$ as the rescaled time. The evolution of a quantum state is then given by

$$\frac{\mathrm{d}}{\mathrm{d}s}|\psi(s)\rangle = -\mathrm{i}TH(s). \tag{1}$$

*Contact author: bojan.zunkovic@fri.uni-lj.si

Published by the American Physical Society under the terms of the Creative Commons Attribution 4.0 International license. Further distribution of this work must maintain attribution to the author(s) and the published article's title, journal citation, and DOI.

By initializing the system in the ground state of H_0, and if the annealing time T is sufficiently large (i.e., under the quantum adiabatic condition [1]), the time-evolved state $|\psi(s)\rangle$ remains close to the ground state $|\psi_0(s)\rangle$ of the instantaneous Hamiltonian $H(s)$. Since the exact description of $|\psi(s)\rangle$ is often challenging, we may approximate its real-time evolution with a variational state $|\psi_x^{\rm VS}(s)\rangle$ constrained to a manifold $\mathcal{M}$ defined by a set of variational parameters x. Its time dependence is fully determined by the variational parameters $x = x(s)$, evolved with the Lagrangian action variational principle [24]. Let us assume that the initial state, namely $|\psi(0)\rangle = |\psi_0(0)\rangle$, lies within the variational manifold $\mathcal{M}$. Thus, the exact and variational dynamics share the same initial condition: $|\psi(0)\rangle = |\psi_x^{\rm VS}(0)\rangle = |\psi_0(0)\rangle$. From now on, we introduce the notation $|\psi_0^{\rm VS}(s)\rangle$ for the instantaneous variational ground state, defined as the variational state with minimal variational energy, which is characterized by $x_0 = x_0(s) = \mathrm{argmin}_x \langle\psi_x^{\rm VS}|H(s)|\psi_x^{\rm VS}\rangle$. Under certain hypotheses detailed in the Appendix, the time-dependent variational state $|\psi_x^{\rm VS}(s)\rangle$ remains close to the instantaneous variational ground state, namely $|\psi_x^{\rm VS}(s)\rangle = |\psi_0^{\rm VS}(s)\rangle + |\delta\psi(s)\rangle$, where $\|\delta\psi(s)\|_2 = \mathcal{O}(1/T)$, for $s \in [0,1]$. If the target ground state belongs to the manifold, i.e., $|\psi_0(1)\rangle = |\psi_0^{\rm VS}(1)\rangle$, then the *variational* state converges to the target ground state at $s = 1$, for large values of T. In practice, we shall consider a low-entanglement manifold and classical initial and final (target) states.

A more precise statement of the theorem is given in the Appendix. Here, we provide only the physical intuition illustrated in Fig. 1. If $\|\delta\psi(s)\|_2$ is small, its evolution is determined by the linearized time-dependent variational equations that give rise to elliptic trajectories around the instantaneous variational ground state $|\psi_0^{\rm VS}(s)\rangle$. The frequencies $\omega_l > 0$ of the trajectories are determined by the eigenvalues of the linearized evolution map on the manifold $\mathcal{M}$ [25] and represent approximate energy gaps over the ground state. If $1/T \ll \omega_l$, then $|\delta\psi(s)\rangle$ will average to zero in a time window where $|\psi_0^{\rm VS}(s)\rangle$ does not change drastically. Therefore, $|\psi_x^{\rm VS}(s)\rangle$ will follow the instantaneous variational ground state $|\psi_0^{\rm VS}(s)\rangle$ and $\|\delta\psi(s)\|_2$ will remain small during the variational time evolution.

In the following, we consider several examples of increasing complexity, with protocols in the form

$$H(s) = (1-s)H_0 + sH_1 + s(1-s)H_2,$$
$$H_0 = -\sum_{j=1}^{N} \sigma_j^{\rm x}, \tag{2}$$

where we may introduce an additional *catalyst* Hamiltonian H_2. In all cases, we initialize the system in the ground state of H_0 and evaluate the convergence of the variational evolution to the target ground state of H_1 in a total time T.

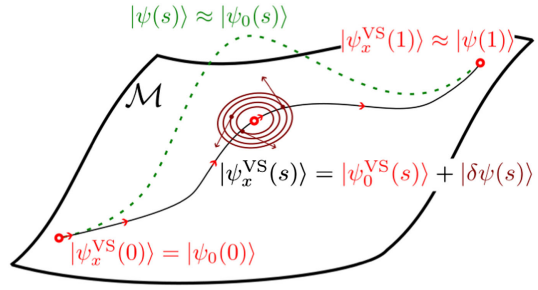

FIG. 1. Schematic representation of the variational ground-state quantum adiabatic theorem. The dashed green line represents the exact quantum adiabatic evolution $|\psi(s)\rangle \approx |\psi_0(s)\rangle$, visiting high-entanglement regions. The solid black line corresponds to the instantaneous variational ground state $|\psi_0^{\rm VS}(s)\rangle$, with the small red arrows indicating that it changes slowly with time. The time-dependent variational state $|\psi_x^{\rm VS}(s)\rangle$ is separated into $|\psi_0^{\rm VS}(s)\rangle$ and their difference $|\delta\psi(s)\rangle$. The latter can be decomposed in the eigenbasis of the linearized evolution map, whose eigenvalues ω_l determine the frequencies of the elliptic trajectories around the instantaneous variational ground state. Since $1/T \ll \omega_l$, the fast dynamics of $|\delta\psi(s)\rangle$ (denoted by long, dark-red arrows) averages to zero, and the time-dependent variational state $|\psi_x^{\rm VS}(s)\rangle$ follows the instantaneous variational ground state $|\psi_0^{\rm VS}(s)\rangle$. When the target ground state of the final Hamiltonian lies within the variational manifold, the time-dependent variational state will converge to it as the annealing time T becomes large.

Two-qubit model—First, we consider a two-qubit model with

$$H_1 = \sigma_1^z\sigma_2^z - 2(\sigma_1^z + \sigma_2^z),$$
$$H_2 = -2A|\Phi\rangle\langle\Phi|, \tag{3}$$

where $|\Phi\rangle = (1/\sqrt{2})(|00\rangle + |11\rangle)$ is a maximally entangled Bell state, and A is a positive constant. The initial and the final ground states are product states where both spins point in the x and z directions, respectively. Therefore, we choose the following product state variational ansatz:

$$|\psi_x^{\rm VS}\rangle = |\psi_{\theta,\phi}\rangle \otimes |\psi_{\theta,\phi}\rangle,$$
$$|\psi_{\theta,\phi}\rangle = \cos(\theta/2)|0\rangle + \sin(\theta/2)\mathrm{e}^{-\mathrm{i}\phi}|1\rangle. \tag{4}$$

The variational manifold given by Eq. (4) is a Kähler manifold [24]. The parameter A determines the entanglement of the ground states of $H(s)$ at intermediate times $0 < s < 1$. In Fig. 2, we show that cases with higher ground-state entanglement at $s = 0.5$ correspond to faster convergence to the variational ground state at the end of the protocol [see Figs. 2(a) and 2(b)]. This example demonstrates that the variational adiabatic evolution can still reach the target ground state, even if the exact quantum adiabatic dynamics would access high-entanglement regions at

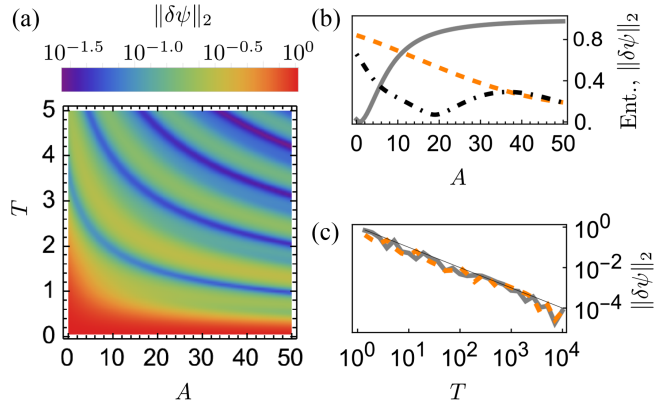

FIG. 2. (a) The final norm $\|\delta\psi(s)\|_2$ at $s = 1$, a measure of the distance between $|\psi_0(1)\rangle$ (the target ground state of H_1) and $|\psi_x^{\rm VS}(1)\rangle$ (the variational state at the end of the annealing). We plot it as a function of the annealing time T and parameter A. (b) Half-system entanglement entropy at intermediate time $s = 0.5$ (gray line) as a function of the parameter A, and the norm $\|\delta\psi(1)\|_2$ for $T = 0.5$ (dashed orange) and $T = 1.5$ (dash-dotted black). Higher entanglement entropy corresponds to smaller values of $\|\delta\psi(1)\|_2$. (c) Scaling of the norm $\|\delta\psi(1)\|_2$ with annealing time T. The thin line corresponds to T^{-1} scaling, the dashed orange line to $A = 0$, and the gray line to $A = 5$.

intermediate times. Figure 2(c) shows the scaling of $\|\delta\psi(1)\|_2 = \mathcal{O}(1/T)$, which is verified regardless of the value of A, as predicted by the variational ground-state adiabatic theorem. This two-qubit model can be extended to a more general bipartite system involving arbitrarily high entanglement at the intermediate ground states of $H(s)$ [24]. Nonetheless, the variational evolution on a product-state manifold is equivalent to the two-qubit case and correctly leads to the target ground state.

Lipkin-Meshkov-Glick model—Next, we consider the integrable Lipkin-Meshkov-Glick (LMG) [26]

$$H_1^{\rm LMG} = -\frac{1}{N}\left(\sum_{i=1}^{N}\sigma_i^z\right)^2 \tag{5}$$

as target Hamiltonian. Similarly to the two-qubit case, we have homogeneous product-state ground states of the initial and final Hamiltonian pointing in the x and z directions, respectively. Therefore, we consider the following mean-field ansatz

$$|\psi_x^{\rm VS}\rangle = |\psi_{\theta,\phi}\rangle^{\otimes N}, \tag{6}$$

with $|\psi_{\theta,\phi}\rangle$ defined as in Eq. (4). The variational manifold is again a Kähler manifold with simple equations of motion for the variational parameters that can be solved numerically for any N [24]. This manifold can be effectively represented as a sphere by considering the expectation value of total spin S, with components

$$S^\alpha = \frac{1}{N}\sum_{i=1}^{N}\langle\psi_{\theta,\phi}|\sigma_i^\alpha|\psi_{\theta,\phi}\rangle, \qquad \alpha = x, y, z. \tag{7}$$

The LMG model crosses a second-order quantum phase transition at $s^* = 1/3$ in the thermodynamic limit. In this limit, states on the manifold exactly describe the dynamics and some properties of the eigenstates [27–29], and the system behaves as a classical spin on the sphere [26]. At finite N, the instantaneous quantum many-body ground state does not belong to the manifold, except at $s = 0, 1$. However, the time-dependent variational state and the instantaneous variational ground state are still represented on the sphere. If the norm of their difference $\|\delta S(s)\|_2 = \|S^{\rm VS}(s) - S_0^{\rm VS}(s)\|_2$ converges to small values at $s = 1$, the variational evolution approximates the exact target ground state.

As shown in [24], the finite N equations of motion on the manifold retain the same structure as in the thermodynamic limit and display a mean-field second-order phase transition at $s^* = (N/3N - 2)$. For $s < s^*$, the instantaneous variational ground state does not depend on s, hence, for any value of T, $\|\delta S(s)\|_2$ oscillates close to its initial value at $s = 0$; for $s > s^*$, the convergence of the time-dependent variational state to the instantaneous variational ground state scales as $\|\delta S(s)\|_2 \sim 1/\sqrt{T}$. Indeed, our assumptions in the variational ground-state quantum adiabatic theorem are not strictly valid in this regime, as $\|\partial_s S_0^{\rm VS}(s)\|$ exhibits a square root divergence at the critical time s^*, leading to a change in the exponent [24].

In Fig. 3, we present a specific case with $N = 4$. Although we deliberately focus on a small system size, distant from the mean-field approximation, the same results apply to any value of N. We start close to the H_0 ground state, with the initial condition shifted 10^{-4} away from the angles $\theta(0) = \pi/2$, $\phi_0 = 0$, which determine a fixed point for all s. In Fig. 3(a) we show a trajectory of the vector $S^{\rm VS}(s)$ (black line) for $T = 500$. We observe fast oscillations around the variational ground-state vector $S_0(s)$ (dashed orange line). These oscillations become faster and the amplitude smaller upon increasing T, as displayed in Fig. 3(c), where we plot $\delta S(s)$ at $s \in [0, 1]$ for three values of T. Consistently, Fig. 3(b) shows the square root dependence of $\|\delta S\|_2$ on T, for $s > s^*$. The jump at $s^* = 0.4$ is related to the mean-field phase transition [24]. Finally, Fig. 3(d) corroborates the agreement of numerical data with the square root scaling, verifying the convergence of the final variational state ($s = 1$) to the target ground state.

Ising spin glass model—Finally, we consider the fully connected random Ising spin glass model with the Hamiltonian

$$H_1^{\rm SG} = \sum_{i,j=1}^{N} J_{ij}\sigma_i^z\sigma_j^z + \sum_{i=1}^{N} h_i\sigma_i^z, \tag{8}$$

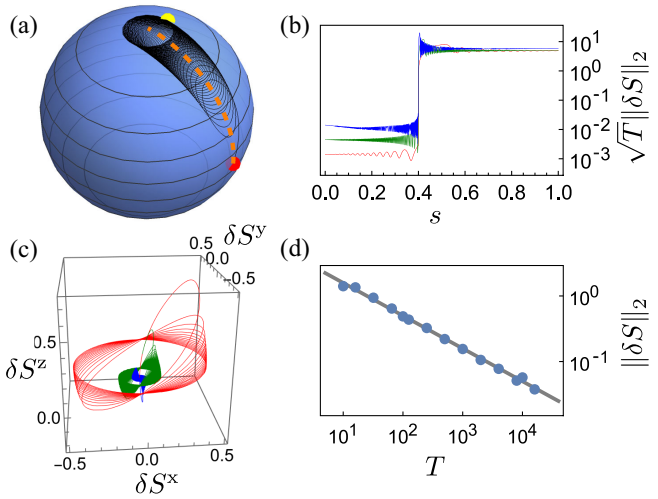

FIG. 3. (a) An example evolution of the vector $S^{\mathrm{VS}}(s)$ (black line) for $N = 4$ and $T = 500$, $s \in [0, 1]$. The red dot corresponds to the initial condition, and the yellow dot corresponds to the final variational state $S^{\mathrm{VS}}(1)$. The dashed orange line shows the *variational* ground state vector $S_0^{\mathrm{VS}}(s)$. (b) Three examples of the evolution of the rescaled norm $\sqrt{T}\|\delta S(s)\|_2$ for $T = 10^2$ (red), $T = 10^3$ (green), and $T = 10^4$ (blue). (c) Convergence of $\delta S(s)$ during the variational time evolution—same data as in panel (b). (d) Scaling of $\|\delta S(1)\|_2$: the solid line represent the predicted $1/\sqrt{T}$; the dots correspond to numerical results.

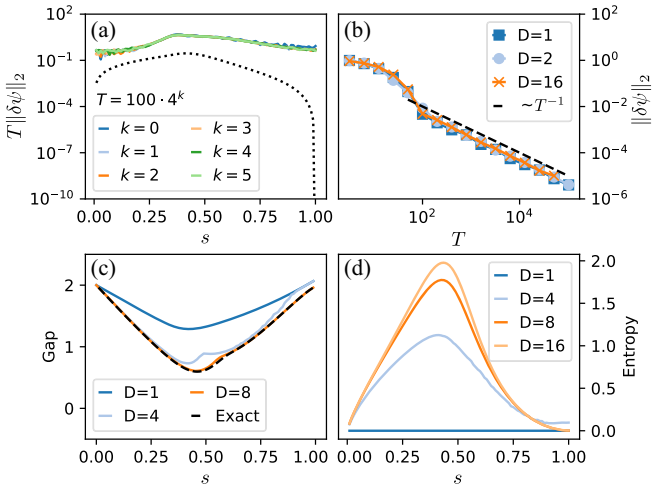

FIG. 4. (a) Convergence of the time-dependent variational state toward the instantaneous variational ground state upon increasing the annealing time T for a particular realization of the Ising spin glass model with $N = 8$. We fix the bond dimension to $D = 1$ and plot $\|\delta\psi(s)\|_2$. The black dotted line shows the norm of the difference between the exact instantaneous ground state and the instantaneous variational ground state. (b) Norm of the difference between the final variational state at $s = 1$, which is $|\psi_x^{\mathrm{VS}}(1)\rangle$, and the exact target ground state of H_1, i.e., $|\psi_0(1)\rangle$, for increasing values of D. Notice that the target state belongs to the MPS manifold with $D = 1$ [see the dotted black line in panel (a), at $s = 1$]. The bond dimension $D = 16$ corresponds to the exact evolution, and the dashed line highlights the predicted scaling $1/T$. (c) The spectral gap calculated from the effective Hamiltonian in the MPS-TDVP evolution for various bond dimensions D. The dashed line corresponds to the exact spectral gap. We set $T = 3200$. (d) Entanglement entropy during the protocol with $T = 3200$ and different bond dimensions.

where $J_{ij} = J_{ji}$ and h_i are random numbers uniformly distributed in the range (0, 1) and $(-0.5, 0.5)$, respectively. Determining the ground state of the model is computationally equivalent to quadratic unconstrained binary optimization and is an NP-complete problem [30].

Here, we use the matrix product-state (MPS) variational ansatz, which enables a systematic increase of maximal entanglement by increasing the bond dimension D. The MPS manifold is a Kähler manifold [15] that enables an inverse-free implementation of the time-dependent variational principle (TDVP) [31] and a simple evaluation of the gap [24].

In Fig. 4(a) we show that the time-dependent variational state $|\psi_x^{\mathrm{VS}}\rangle$ with $D = 1$ converges uniformly, i.e., for all $0 < s \leq 1$, toward the instantaneous variational ground state with the same bond dimension. The expected $1/T$ convergence remains valid upon increasing the bond dimension, as shown in Fig. 4(b). As predicted by our theorem, we obtain the target ground state even by constraining the variational adiabatic evolution to a low-entanglement manifold. The results shown in Fig. 4 refer to a specific disordered instance of the Ising spin glass. Still, we verified their validity on different realizations of the random quenched disorder.

The MPS-TDVP approach enables the efficient estimate of the instantaneous gap through the effective Hamiltonian [24]. In Fig. 4(c), we show the convergence of the effective gap with increasing bond dimension. The exact gap at the protocol's beginning and end is well approximated, even with a small bond dimension. This is expected since the initial and final (target) ground states are product states. In contrast, a correct estimation in the middle of the protocol requires higher bond dimension values. This overall trend reflects the overlap between the exact and the variational ground states [see black dotted line in panel (a), for the case of $D = 1$). Consistently, ground-state entanglement is large in the middle of the protocol, as shown in Fig. 4(d).

In Fig. 5, we present the histogram of the norm $\|\delta\psi(s)\|_2$ for $s = 1$, representing the distance of the final variational state from the exact target ground state, for 100 random realizations of the Hamiltonian in Eq. (8). We observe that for $D = 1$, $D = 2$, $D = 4$, and $D = 8$, approximately 20%, 8%, 2%, and 1% of the instances do not accurately converge to the target ground state for $T = 1600$, i.e., the final norm $\|\delta\psi(1)\|_2 > 0.999$. This is related to spurious first-order phase transitions for the variational parameters, which appear more likely for smaller values of D, namely for lower-dimensional manifolds (see Ref. [24] for details). However, in all cases, we were able to recover the correct ground state with an additional density matrix renormalization group

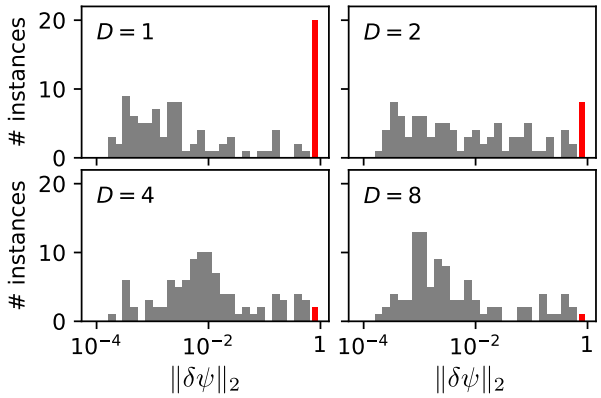

FIG. 5. Histogram of the norm $\|\delta\psi(1)\|_2$ at the end of the annealing protocol with $D = 1$, 2, 4, 8, and $T = 1600$. The histogram is computed from 100 random realizations of the final Hamiltonian H_1. We fixed $N = 8$. The red bars correspond to instances with values larger than 0.999.

(DMRG) run at the end of the protocol. Even if the final variational state has a small overlap with the target state, it may serve as a warmup for DMRG, leading to better convergence than random initializations.

Conclusions and outlook—Our theorem states that, given a quantum adiabatic protocol with sufficiently slow evolution and a variational manifold, the time-dependent variational state remains close to the instantaneous variational ground state, provided the hypotheses are satisfied. If the initial and final states lie within a classically simulable variational manifold, under the theorem's assumptions, this could open up a new promising computational paradigm: an efficient quantum-inspired classical algorithm performs the manifold evolution as in Fig. 1, finally reaching the target state.

This approach has been proven valid for low-entanglement variational manifolds and various classical target Hamiltonians, e.g., for a spin glass, resulting in numerical outcomes consistent with the predicted scaling. Selecting an appropriate manifold, such as the MPS manifold with a larger bond dimension, can enhance the final results and decrease the annealing time needed to find the target state. We also stress that this approach could be extended to quantum many-body ground-state preparation. In this case, provided that the hypothesis of the theorem holds, it is essential to select the variational manifold carefully, ensuring it captures the entanglement of the target state.

The proposed variational adiabatic computing scheme represents a novel classical paradigm, distinct from simulated annealing and simulated quantum annealing, which rely on Monte Carlo sampling. We anticipate that its ultimate effectiveness in solving complex classical optimization problems and other applications may be linked to two natural extensions of our Letter. Firstly, our variational adiabatic strategy could be extended to imaginary or complex time. This would result in an effective cooling during the adiabatic evolution, which can further improve the results. Various combinations with DMRG are also possible. Secondly, we plan to examine different variational manifolds, such as PEPS [32] or neural-network quantum states [33–36]. Another promising approach involves selecting a parametrized quantum circuit as the variational manifold, which can be iteratively trained to approximate the instantaneous adiabatic state on real quantum hardware.

These advances could enable tackling more challenging problems and comparing the performance on larger instances with state-of-the-art classical methods or experimental implementations of quantum annealing. Furthermore, the variational quantum adiabatic paradigm may be adapted to finding excited states of the energy spectrum, extending its application beyond ground-state search. Some substantial practical benefits compared to a fully quantum adiabatic evolution are already evident, e.g., access to the exact variational quantum state, which enables boosting an exceedingly small probability of finding the correct solution (such as $\approx 10^{-12}$) to almost one: this can be accomplished via DMRG on the final variational state, or similar methods.

From a theoretical perspective, the challenge of identifying a practical sufficient condition for the applicability of the variational adiabatic theorem remains open. Nonetheless, our methods could be readily applied to various contexts traditionally studied within the framework of quantum annealing. Examples include the generalized Landau-Zener problem [37], mechanisms to circumvent slowdown for adiabatic quantum computation [1], and the nonadiabatic evolution [38]. Moreover, it would be possible to employ the manifold simulations to approximately estimate the position of the minimum adiabatic gap. Therefore, variational adiabatic evolution appears to be a novel and robust classical baseline for benchmarking quantum protocols and a valuable tool for developing novel classical algorithms inspired by quantum methods or improving existing quantum annealing algorithms [39,40].

Acknowledgments—B. Z. was funded by Slovenian Research and Innovation agency (ARIS) project No. J1-2480, ARIS research program P2-0209 Artificial Intelligence and Intelligent Systems (2022–2024), and the University of Ljubljana Project under Contract No. SN-ZRD/22-27/0510. P. T. acknowledges the project CQES of the Italian Space Agency (ASI) for having supported his research (Grant No. 2023-46-HH.0). G. P. acknowledges financial support from the QuantERA II Programme STAQS project that has received funding from the European Union's H2020 research and innovation program under Grant Agreement No. 101017733. G. L. was supported by ANR-22-CPJ1-0021-01 and ERC Starting Grant No. 101042293 (HEPIQ). M. C. acknowledges support from the PNRR MUR project PE0000023-NQSTI and by the PRIN 2022 (2022R35ZBF) - PE2 - "ManyQLowD." Computational resources were provided by SLING, a Slovenian national supercomputing network.

[1] T. Albash and D. A. Lidar, Adiabatic quantum computation, Rev. Mod. Phys. **90**, 015002 (2018).

[2] D. Aharonov, W. Van Dam, J. Kempe, Z. Landau, S. Lloyd, and O. Regev, Adiabatic quantum computation is equivalent to standard quantum computation, SIAM Rev. **50**, 755 (2008).

[3] A. Mizel, D. A. Lidar, and M. Mitchell, Simple proof of equivalence between adiabatic quantum computation and the circuit model, Phys. Rev. Lett. **99**, 070502 (2007).

[4] B. Apolloni, C. Carvalho, and D. De Falco, Quantum stochastic optimization, Stoch. Proc. Appl. **33**, 233 (1989).

[5] M. W. Johnson *et al.*, Quantum annealing with manufactured spins, Nature (London) **473**, 194 (2011).

[6] S. Yarkoni, E. Raponi, T. Bäck, and S. Schmitt, Quantum annealing for industry applications: Introduction and review, Rep. Prog. Phys. **85**, 104001 (2022).

[7] E. Crosson and A. W. Harrow, Simulated quantum annealing can be exponentially faster than classical simulated annealing, in *2016 IEEE 57th Annual Symposium on Foundations of Computer Science (FOCS)* (IEEE, 2016), pp. 714–723, 10.1109/FOCS.2016.81.

[8] G. Carleo, B. Bauer, and M. Troyer, Simulating adiabatic quantum computation with a variational approach, arXiv:2403.05147.

[9] M. Cerezo, M. Larocca, D. García-Martín, N. L. Diaz, P. Braccia, E. Fontana, M. S. Rudolph, P. Bermejo, A. Ijaz, S. Thanasilp, E. R. Anschuetz, and Z. Holmes, Does provable absence of barren plateaus imply classical simulability? Or, why we need to rethink variational quantum computing, arXiv:2312.09121.

[10] P. J. D. Crowley, T. Đurić, W. Vinci, P. A. Warburton, and A. G. Green, Quantum and classical dynamics in adiabatic computation, Phys. Rev. A **90**, 042317 (2014).

[11] J. Chen, E. M. Stoudenmire, and S. R. White, Quantum fourier transform has small entanglement, PRX Quantum **4**, 040318 (2023).

[12] Z.-Y. Han, J. Wang, H. Fan, L. Wang, and P. Zhang, Unsupervised generative modeling using matrix product states, Phys. Rev. X **8**, 031012 (2018).

[13] B. Žunkovič, Deep tensor networks with matrix product operators, Quantum Mach. Intell. **4**, 21 (2022).

[14] B. Žunkovič, Positive unlabeled learning with tensor networks, Neurocomputing **552**, 126556 (2023).

[15] J. Haegeman, M. Mariën, T. J. Osborne, and F. Verstraete, Geometry of matrix product states: Metric, parallel transport, and curvature, J. Math. Phys. (N.Y.) **55**, 021902 (2014).

[16] J. Biamonte and V. Bergholm, Tensor networks in a nutshell, arXiv:1708.00006.

[17] W. Huggins, P. Patil, B. Mitchell, K. B. Whaley, and E. M. Stoudenmire, Towards quantum machine learning with tensor networks, Quantum Sci. Technol. **4**, 024001 (2019).

[18] G. Lami, P. Torta, G. E. Santoro, and M. Collura, Quantum annealing for neural network optimization problems: A new approach via tensor network simulations, SciPost Phys. **14**, 117 (2023).

[19] R. Sreedhar, P. Vikstål, M. Svensson, A. Ask, G. Johansson, and L. García-Álvarez, The quantum approximate optimization algorithm performance with low entanglement and high circuit depth, arXiv:2207.03404.

[20] E. Farhi, J. Goldstone, and S. Gutmann, A quantum approximate optimization algorithm, arXiv:1411.4028.

[21] Y. Chen, L. Zhu, C. Liu, N. J. Mayhall, E. Barnes, and S. E. Economou, How much entanglement do quantum optimization algorithms require?, arXiv:2205.12283.

[22] M. Dupont, N. Didier, M. J. Hodson, J. E. Moore, and M. J. Reagor, Entanglement perspective on the quantum approximate optimization algorithm, Phys. Rev. A **106**, 022423 (2022).

[23] R. Shaydulin *et al.*, Evidence of scaling advantage for the quantum approximate optimization algorithm on a classically intractable problem, Sci. Adv. **10**, eadm6761 (2024).

[24] See Supplemental Material at http://link.aps.org/supplemental/10.1103/PhysRevLett.134.130601 for a brief summary of the time-dependent variational principle (TDVP) and for analytical calculations and additional numerical results on the models discussed in the main text: a bipartite system, the Lipkin-Meshkov-Glick (LMG) model, the Ising spin glass model.

[25] L. Hackl, T. Guaita, T. Shi, J. Haegeman, E. Demler, and J. I. Cirac, Geometry of variational methods: Dynamics of closed quantum systems, SciPost Phys. **9**, 048 (2020).

[26] H. J. Lipkin, N. Meshkov, and A. Glick, Validity of many-body approximation methods for a solvable model:(I). Exact solutions and perturbation theory, Nucl. Phys. **62**, 188 (1965).

[27] E. Granet, Exact mean-field solution of a spin chain with short-range and long-range interactions, SciPost Phys. **14**, 133 (2023).

[28] B. Žunkovič and P. Ribeiro, Mean-field approach to mid-spectrum eigenstates of long-range interacting quantum systems, arXiv:2310.09803.

[29] B. Žunkovič and A. Zegarra, Mean-field dynamics of an infinite-range interacting quantum system: Chaos, dynamical phase transition, and localization, Phys. Rev. B **109**, 064309 (2024).

[30] F. Barahona, On the computational complexity of ising spin glass models, J. Phys. A **15**, 3241 (1982).

[31] J. Haegeman, C. Lubich, I. Oseledets, B. Vandereycken, and F. Verstraete, Unifying time evolution and optimization with matrix product states, Phys. Rev. B **94**, 165116 (2016).

[32] J. I. Cirac, D. Pérez-García, N. Schuch, and F. Verstraete, Matrix product states and projected entangled pair states: Concepts, symmetries, theorems, Rev. Mod. Phys. **93**, 045003 (2021).

[33] G. Carleo and M. Troyer, Solving the quantum many-body problem with artificial neural networks, Science **355**, 602 (2017).

[34] M. Schmitt and M. Heyl, Quantum many-body dynamics in two dimensions with artificial neural networks, Phys. Rev. Lett. **125**, 100503 (2020).

[35] G. Lami, G. Carleo, and M. Collura, Matrix product states with backflow correlations, Phys. Rev. B **106**, L081111 (2022).

[36] M. Hibat-Allah, E. M. Inack, R. Wiersema, R. G. Melko, and J. Carrasquilla, Variational neural annealing, Nat. Mach. Intell. **3**, 952 (2021).

[37] S. Brundobler and V. Elser, S-matrix for generalized Landau-Zener problem, J. Phys. A **26**, 1211 (1993).

[38] E. Crosson, E. Farhi, C. Y.-Y. Lin, H.-H. Lin, and P. Shor, Different strategies for optimization using the quantum adiabatic algorithm, arXiv:1401.7320.
[39] C. Mc Keever and M. Lubasch, Towards adiabatic quantum computing using compressed quantum circuits, PRX Quantum **5**, 020362 (2024).
[40] G. Pecci, R. Wang, P. Torta, G. B. Mbeng, and G. Santoro, Beyond quantum annealing: Optimal control solutions to maxcut problems, Quantum Sci. Technol. **9**, 045013 (2024).
[41] J. Burke, Lecture notes: Linear ode, https://sites.math.washington.edu/~burke/crs/555/555_notes/linear.pdf (2015) (accessed: 2023-11-29).
[42] A. Mostafazadeh, Pseudo-Hermitian representation of quantum mechanics, Int. J. Geom. Methods Mod. Phys. **07**, 1191 (2010).
[43] A. Mostafazadeh, Pseudo-Hermiticity versus PT symmetry: The necessary condition for the reality of the spectrum of a non-Hermitian Hamiltonian, J. Math. Phys. (N.Y.) **43**, 205 (2002).
[44] D. C. Brody, Biorthogonal quantum mechanics, J. Phys. A **47**, 035305 (2013).
[45] A. Mostafazadeh, Time-dependent pseudo-Hermitian Hamiltonians and a hidden geometric aspect of quantum mechanics, Entropy **22**, 471 (2020).
[46] G. Nenciu and G. Rasche, On the adiabatic theorem for nonself-adjoint Hamiltonians, J. Phys. A **25**, 5741 (1992).
[47] N. Silberstein, J. Behrends, M. Goldstein, and R. Ilan, Berry connection induced anomalous wave-packet dynamics in non-Hermitian systems, Phys. Rev. B **102**, 245147 (2020).
[48] S. Cheniti, W. Koussa, A. Medjber, and M. Maamache, Adiabatic theorem and generalized geometrical phase in the case of pseudo-Hermitian systems, J. Phys. A **53**, 405302 (2020).

End Matter

Appendix: Variational ground-state quantum adiabatic theorem—

Theorem 1 Assume a time-dependent Hamiltonian $H(t)$ whose instantaneous ground state $|\psi_0(t)\rangle$ at time $t=0$ lies in the variational manifold $\mathcal{M}$. Introduce the rescaled time $s=t/T$, where T is the annealing time determining the inverse rate of change of $H(t)$. Consider a variational state $|\psi_x^{\mathrm{VS}}(s)\rangle \in \mathcal{M}$ whose time dependence is fully determined by the variational parameters $x=x(s)$. Starting in the initial ground state $|\psi_x^{\mathrm{VS}}(0)\rangle = |\psi_0(0)\rangle$, the variational parameters are evolved with the (Lagrangian action) variational principle

$$\frac{1}{T}\frac{\mathrm{d}}{\mathrm{d}s}x = \mathcal{X}(x), \qquad \mathcal{X}(x) = -\Omega^{\mu,\nu}\partial_\nu E_s(x). \tag{A1}$$

The resulting dynamics on the manifold can be decomposed as $|\psi_x^{\mathrm{VS}}(s)\rangle = |\psi_0^{\mathrm{VS}}(s)\rangle + |\delta\psi(s)\rangle$, where $|\psi_0^{\mathrm{VS}}(s)\rangle$ denotes the instantaneous variational ground state characterized by $x_0 = x_0(s)$. If the linearized symplectic generator $K(s)$ defined by

$$K^\mu{}_\nu(s) = \partial_{x^\nu}\mathcal{X}^\mu\Big|_{x=x_0(s)} \tag{A2}$$

satisfies the adiabatic conditions for η-pseudo-Hermitian quantum evolution, then

$$\|\delta\psi(s)\|_2 = \mathcal{O}\left(\frac{1}{T}\right) \quad \text{for } s\in[0,1]. \tag{A3}$$

More precisely, if $\delta x(s) = x(s) - x_0(s)$, we obtain

$$\|\delta x(s)\|_{\eta(s)} \sim \kappa\left(\frac{1}{T}\right) \quad \text{for } s\in[0,1], \tag{A4}$$

where the norm is calculated with respect to the pseudoinner product and

$$\kappa = \frac{2\max_{s,s',j}\left|\mathrm{e}^{-\mathrm{i}(\Gamma_j(s)-\Gamma_j(s'))}\right|\max_s\|\dot{x}_0(s)\|_{\eta(s)}}{\min_{s,i}|\omega_i(s)|}, \tag{A5}$$

with $\Gamma_j(s)$ denoting the generalized geometric phase. If the previous term does not diverge, the time-dependent variational state closely follows the instantaneous variational ground state.

Proof Let us consider the time evolution of the difference between the parameters of the time-dependent variational state and those of the instantaneous variational ground state

$$\delta x(s) = x(s) - x_0(s). \tag{A6}$$

The equations of motion for $\delta x(s)$ are

$$\frac{1}{T}\partial_s(x_0(s)+\delta x(s)) = \mathcal{X}(x_0(s)+\delta x(s)), \tag{A7}$$

Initially, by hypothesis, we have $\delta x(0)=0$. Our strategy is to show that the pseudonorm of the difference $\|\delta x(s)\|_{\eta(s)}$ remains small during the adiabatic evolution.

We start by linearizing the dynamics in Eq. (A7) in a local neighborhood of $x_0(s)$,

$$\frac{1}{T}\partial_s(x_0(s)+\delta x(s)) \approx \mathcal{X}(x_0(s)) + K(s)\delta x(s), \tag{A8}$$

where $K^\mu{}_\nu(s) = \partial_{x^\nu}\mathcal{X}^\mu|_{x=x_0(s)}$. Since the instantaneous variational ground state is a stationary point of the Lagrangian action variational evolution [25], we have $\mathcal{X}(x_0(s)) = 0$ and

$$\partial_s\delta x(s) = TK(s)\delta x(s) - \partial_s x_0(s). \tag{A9}$$

We find the solution of the above inhomogeneous first-order differential equation in terms of the fundamental matrix satisfying [41]

$$\partial_s U(s) = TK(s)U(s). \tag{A10}$$

A formal solution to Eq. (A10) is determined by a time-ordered exponential

$$U(s) = \mathcal{T}_{\leftarrow} \mathrm{e}^{\int_0^s TK(u)\mathrm{d}u}. \tag{A11}$$

We write $\delta x(s)$ as a sum of the homogeneous and the particular solution of Eq. (A9). Because of the initial condition $\delta x(s=0)=0$, the homogeneous part of the solution vanishes since $\delta x_{\mathrm{h}}(s) = U(s)\delta x(0) = 0$. The particular part, therefore, determines the final solution,

$$\delta x(s) = \delta x_{\mathrm{P}}(s) = -U(s)\int_0^s U^{-1}(u)\dot{x}_0(u)\mathrm{d}u, \tag{A12}$$

where we introduced the notation $\dot{x}_0(s) = \partial_s x_0(s)$

To further simplify the expression Eq. (A12), we use the structure of the symplectic generator K, which is always diagonalizable and whose eigenvalues appear in conjugate imaginary pairs [25]. Consequently, $\mathrm{i}K$ has real eigenvalues implying the existence of a strictly positive definite metric operator η such that [42,43]

$$(\mathrm{i}K)^\dagger \eta = \eta(\mathrm{i}K). \tag{A13}$$

The above relation implies that $\mathrm{i}K$ is Hermitian with respect to the pseudoinner product

$$\langle\psi|\phi\rangle_\eta = \langle\psi|\eta|\phi\rangle. \tag{A14}$$

Therefore, Eq. (A10) is a real-time Schrödinger equation with a pseudo-Hermitian Hamiltonian $\mathrm{i}K$ [42,44,45]. Although we shall adopt the standard Dirac notation, notice that the operator $\mathrm{i}K$ and the parameter vectors introduced in (A6) act on the variational manifold $\mathcal{M}$. We can find the left $\{|\tilde{\omega}_i(s)\rangle\}$ and right $\{|\omega_i(s)\rangle\}$ eigenvectors of $\mathrm{i}K(s)$ with the corresponding eigenvalues $\omega_i(s)$, namely $-\mathrm{i}K(s)^\dagger|\tilde{\omega}_i(s)\rangle = \omega_i(s)|\tilde{\omega}_i(s)\rangle$ and $\mathrm{i}K(s)|\omega_i(s)\rangle = \omega_i(s)|\omega_i(s)\rangle$. The left and right eigenvectors are related via

$$|\tilde{\omega}_i(s)\rangle = \eta(s)|\omega_i(s)\rangle \tag{A15}$$

and satisfy the biorthonormality condition

$$\begin{aligned}\langle\omega_i(s)|\tilde{\omega}_j(s)\rangle &= \langle\omega_i(s)|\eta(s)|\omega_j(s)\rangle \\ &= \langle\omega_i(s)|\omega_j(s)\rangle_{\eta(s)} = \delta_{i,j}.\end{aligned} \tag{A16}$$

Recently, a pseudo-Hermitian generalization of quantum mechanics has been worked out [42,44]. Since our linearized homogeneous equation Eq. (A10) is exactly a Schrödinger equation for the pseudo-Hermitian Hamiltonian $\mathrm{i}K$ we apply the adiabatic theorem for pseudo-Hermitian quantum dynamics [42,45–47]. We assume

$$\frac{1}{T}\max_{s\in[0,1]}\frac{|\langle\tilde{\omega}_i(s)|\partial_s K(s)|\omega_j(s)\rangle|}{|\omega_i(s)-\omega_j(s)|^2} \ll 1, \quad \forall i \neq j. \tag{A17}$$

According to the pseudo-Hermitian quantum adiabatic theorem [45,47,48], we have

$$\begin{aligned}U(s)|\omega_j(0)\rangle &\approx \mathrm{e}^{\mathrm{i}T\Phi_j(s)}\mathrm{e}^{\mathrm{i}\Gamma_j(s)}|\omega_j(s)\rangle, \\ U^{-1}(s)|\omega_j(s)\rangle &\approx \mathrm{e}^{-\mathrm{i}T\Phi_j(s)}\mathrm{e}^{-\mathrm{i}\Gamma_j(s)}|\omega_j(0)\rangle,\end{aligned} \tag{A18}$$

where

$$\begin{aligned}\Phi_j(s) &= \int_0^s \omega_j(u)\mathrm{d}u, \\ \Gamma_j(s) &= \frac{1}{2}\int_0^s (\langle\dot{\tilde{\omega}}_j(u)|\omega_j(u)\rangle - \langle\omega_j(u)|\dot{\tilde{\omega}}_j(u)\rangle)\mathrm{d}u.\end{aligned}$$

The key difference from the standard Hermitian adiabatic theorem is that the geometric phase $\Gamma_j(s)$ does not vanish for open paths and is not necessarily real. Consequently, it can contribute to the global phase and change the norm of the eigenstates. However, the generalized geometric phase does not depend on the total evolution time T; hence, it contributes only as a prefactor to the final result.

Since the left and right eigenvectors satisfy the completeness relation $\mathbb{1} = \sum_j |\omega_j(s)\rangle\langle\tilde{\omega}_j(s)|$, we can expand the inhomogeneous vector term as

$$|\dot{x}_0(s)\rangle = \sum_j |\omega_j(s)\rangle\langle\tilde{\omega}_j(s)|\dot{x}_0(s)\rangle, \tag{A19}$$

where we exploit the bra-ket notation. After inserting the expansion Eq. (A19) into the expression in Eq. (A12) and using the pseudo-Hermitian adiabatic approximation, we find

$$|\delta x(s)\rangle \approx -\sum_j \int_0^s \mathrm{e}^{\mathrm{i}T(\Phi_j(s)-\Phi_j(u))} g_j(s,u)\mathrm{d}u|\omega_j(s)\rangle, \tag{A20}$$

where

$$g_j(s,u) = \mathrm{e}^{\mathrm{i}(\Gamma_j(s)-\Gamma_j(u))}\langle\tilde{\omega}_j(u)|\dot{x}_0(u)\rangle. \tag{A21}$$

We aim to bound the norm $\|\delta x(s)\|_\eta$. Because of the biorthogonality relation, by using the pseudoinner product definition in Eq. (A14), we obtain

$$\langle\delta x(s)|\delta x(s)\rangle_{\eta(s)} \approx \sum_j \left|\int_0^s \mathrm{e}^{-\mathrm{i}T\Phi_j(u)} g_j(s,u)\mathrm{d}u\right|^2. \tag{A22}$$

We assume that $\omega_i(s)$, which represent the approximations of the excitation energies over the ground state, do not vanish. Now we can evaluate the integral in Eq. (A22) using integration by parts and neglecting the second part since it is asymptotically smaller for large T,

$$\|\delta x(s)\|^2_{\eta(s)} \approx \sum_j \left| \frac{\mathrm{i}}{T} \frac{g_j(s,u)}{\omega_j(u)} \mathrm{e}^{-\mathrm{i}T \int_0^u \omega_j(u')\mathrm{d}u'} \Big|_{u=0}^{u=s} \right|^2.$$

After some algebra, we find the following upper bound for $\|\delta x(s)\|^2_{\eta(s)}$,

$$\left(\frac{2\max_{s,s',j} |\mathrm{e}^{-\mathrm{i}(\Gamma_j(s)-\Gamma_j(s'))}| \max_s \|\dot{x}_0(s)\|_{\eta(s)}}{T \min_{s,i} |\omega_i(s)|} \right)^2. \quad \text{(A23)}$$

In cases where $\omega_i(s)$ vanishes, we would have a degenerate ground state, and the assumptions of the pseudo-Hermitian adiabatic theorem would not be valid. The same occurs if $\|\dot{x}_0(s)\|_{\eta(s)}$ diverges at some critical point s_c, due to a spurious phase transition that may appear if the manifold is not sufficiently expressive [24].

In conclusion, let us write the time-dependent variational state as $|\psi_x^{\mathrm{VS}}(s)\rangle = |\psi_0^{\mathrm{VS}}(s)\rangle + |\delta\psi(s)\rangle$, where $|\psi_0^{\mathrm{VS}}(s)\rangle$ is the variational ground state. If the variational parameters x are close to the ground-state variational parameters x_0, we can perform a first-order expansion centered on x_0, leading to

$$|\delta\psi\rangle = \sum_\mu \partial_{x^\mu} |\psi_x^{\mathrm{VS}}\rangle|_{x=x_0} \delta x_j, \quad \text{(A24)}$$

where we dropped the s dependence for conciseness. The inner product of partial derivatives defines the real-valued metric $\mathbf{g}$ and the symplectic form $\boldsymbol{\omega}$ on the variational manifold [25],

$$\langle \partial_{x^\mu} \psi_x^{\mathrm{VS}} | \partial_{x^\nu} \psi_x^{\mathrm{VS}} \rangle = \frac{1}{2}(g_{\mu,\nu} + \mathrm{i}\omega_{\mu,\nu}). \quad \text{(A25)}$$

Finally, by restoring the s dependence, we have

$$\begin{aligned} \|\delta\psi(s)\|_2^2 &= \frac{1}{2} \delta x(s)^T (\mathbf{g}(s) + \mathrm{i}\boldsymbol{\omega}(s)) \delta x(s) \\ &\leq \frac{|\lambda_{\max}(s)|}{2} \|\delta x(s)\|_2^2 \\ &\leq \frac{|\lambda_{\max}(s)|}{2\Lambda_{\min}(s)} \|\delta x(s)\|^2_{\eta(s)}, \end{aligned} \quad \text{(A26)}$$

where $\lambda_{\max}$ is the eigenvalue with the maximum modulus of the Hermitian matrix $(\mathbf{g} + \mathrm{i}\boldsymbol{\omega})$, and $\Lambda_{\min}$ is the minimum eigenvalue of the positive definite metric operator η. If the assumptions of the theorem are verified, this leads to $\|\delta\psi(s)\|_2 = \mathcal{O}(1/T)$, for $s \in [0, 1]$. ■